bioRxiv preprint doi: https://doi.org/10.1101/695734; this version posted July 8, 2019. The copyright holder for this preprint (which was not certified by peer review) is the author/funder, who has granted bioRxiv a license to display the preprint in perpetuity. It is made available under aCC-BY-ND 4.0 International license.

Microscale interactions between immigrant bacteria and plant leaf microbiota as revealed by live imaging

Shifra Steinberg[1]*, Michael Beitelman[1]*, Maor Grinberg[1], Julianna Peixoto[1,2], Tomer Orevi[1], Nadav Kashtan[1†]

[1] Department of Plant Pathology and Microbiology, Robert H. Smith Faculty of Agriculture, Food, and Environment, Hebrew University, Rehovot, 76100 Israel

[2] Current address: Laboratory of Enzymology, Department of Cellular Biology, Biological Sciences Institute, University of Brasilia, Brasilia, 70910-900, DF, Brazil

* These authors contributed equally to this work.

† Corresponding author: Nadav Kashtan nadav.kashtan@mail.huji.ac.il

Abstract

The phyllosphere – the aerial parts of plants – is an important microbial habitat that is home to diverse microbial communities. The spatial organization of bacterial cells on leaf surfaces is non-random and correlates with leaf microscopic features. Yet the role of microscale interactions between cells therein is not well-understood. Here, we ask how interactions between immigrant bacteria and resident microbiota affect the spatial organization of the combined population. By means of live imaging on a simplified *in vitro* system, we studied the microscale spatial organization of the plant pathogen *Pseudomonas syringae* B728a and the bio-control agent *P. fluorescens* A506 when introduced to both native and non-native leaf microbiota (bean and pear). We revealed that both strains preferentially attach to the surface in locations adjacent to microbiota aggregates. Interestingly, preferential attachment of microbiota cells near newly formed *P. fluorescens* aggregates was also observed. Our results indicate that two-way immigrant bacteria – resident microbiota interactions affect the microscale spatial organization of leaf microbial communities; and that preferential attachment – previously suggested as a general strategy that increases fitness under periodic stress – is a common surface colonization strategy. The implications of this study are likely relevant to other surface-associated microbial habitats.

Introduction

Leaf surfaces constitute a huge microbial habitat that is inhabited by diverse microbial populations including bacteria, yeast, and filamentous fungi (1-9). Bacteria are the most abundant organism among the leaf microbiota (3). The bacterial population of a

bioRxiv preprint doi: https://doi.org/10.1101/695734; this version posted July 8, 2019. The copyright holder for this preprint (which was not certified by peer review) is the author/funder, who has granted bioRxiv a license to display the preprint in perpetuity. It is made available under aCC-BY-ND 4.0 International license.

typical leaf is comprised of hundreds of species of diverse phyla (3, 6, 10). Bacterial cell densities on leaves may reach around 10^5-10^6 cells per cm^2, and cells are observed both as solitary cells and as multi-cellular aggregates often comprised of several species (3, 11-13). The spatial organization of cells on the leaf surface is not uniform and bacterial colonization correlates with the leaf's microscopic heterogeneity. Bacterial cells and aggregates were shown to more likely colonize veins, trichome bases, stomata, and the cavities between epidermal cells (1, 8, 11, 14-16). It is thus clear that leaf microscale heterogeneity plays an important role in determining the microscale microbial organization on leaf surfaces. However, it is not well-understood whether, how, and at which spatial scales, cell-to-cell interactions affect the microscale spatial organization of leaf microbiota cells.

Mapping the spatial organization of the leaf microbiota population at single-cell resolution is a challenge. Thus far, it has been done by means of microscopy of leaf-inoculation experiments involving a small number of interacting strains (15, 17, 18) and through analysis of the natural microbiota, which was limited to a low taxonomic resolution (13). Even if one could map the microscale organization of cells, it would be hard to assess how much of this organization is due to cell-to-cell interactions, as leaf surface heterogeneity may mask this information.

Several studies have sought to understand the microscale colonization patterns of immigrant bacteria upon arrival to a new leaf, and how this organization affects cell survival. The fate of individual bacteria was found to depend upon variation in local carrying capacity (19, 20). Moreover, aggregates of resident bacteria were shown to facilitate survival of immigrant bacteria on leaf surfaces (21, 22). The majority of these studies were not based on continuous live imaging, therefore they could not clearly indicate whether cells preferentially attached to resident bacterial aggregates, or if cells that randomly attached near or onto aggregates had better survival rates.

In a previous study, we suggested that preferential attachment (PA) of cells to existing aggregates can improve survival in environments exposed to periodic stress (23). That work was based on an individual-based modeling approach that used computer simulations of foraging planktonic cells colonizing a surface under alternating wet-dry cycles. Here we asked whether PA is observed experimentally, using two well-studied

bioRxiv preprint doi: https://doi.org/10.1101/695734; this version posted July 8, 2019. The copyright holder for this preprint (which was not certified by peer review) is the author/funder, who has granted bioRxiv a license to display the preprint in perpetuity. It is made available under aCC-BY-ND 4.0 International license.

phyllospheric model strains introduced to natural leaf microbiota extracted from fresh leaves.

Because foliar pathogens typically spend some time as epiphytes before penetrating the leaf interior and causing a disease, it is important to understand what they do and how they survive on the leaf surface. Little is known about how microscale interactions with the natural microbiota affect organization of an immigrant pathogen. In addition, the early colonization of biocontrol agents is also of great interest. As these agents' establishment on the leaf is desired, it is of interest to understand how interactions with the native microbiota affect their colonization.

To focus on cell-to-cell interactions and to exclude the impact of the leaf surface heterogeneity, we used a simplified experimental system based on glass-bottom multi-well plates. Two model strains were used as immigrant bacteria: *Pseudomonas syringae* B728a (*Ps* B728a) and *P. fluorescens* A506 (*Pf* A506). *Ps* B728a is a foliar pathogen model strain that is the cause of brown spot on bean (24-26). *Pf* A506 is a model bio-control agent that is used against *Erwinia amylovora*: the cause of fire blight disease in pear and apple (27, 28). These two strains were introduced to natural microbiota extracted from the surface of fresh leaves. Live imaging microscopy was used to track the microscale spatial organization of both immigrant bacteria and resident microbiota for 13 hours post inoculation. Analyses of the spatiotemporal organization of the combined population of the immigrant cells and the resident microbiota on surfaces at micrometer and single-cell resolutions enabled us to reveal non-random spatial organization patterns of immigrant cells with respect to microbiota; and those of microbiota cells with respect to immigrant bacteria aggregates.

Materials and Methods

Strains and culture conditions

Pseudomonas syringae B728a (25) and *Pseudomonas fluorescens* A506 (28), isolated respectively from green bean and pear leaves, were obtained from Steven E. Lindow, UC Berkeley. *Ps* B728a carried the pKT-TRP plasmid for a constitutive GFP expression(21), whereas *Pf* A506 was transformed using the Tn7 system (29) to

bioRxiv preprint doi: https://doi.org/10.1101/695734; this version posted July 8, 2019. The copyright holder for this preprint (which was not certified by peer review) is the author/funder, who has granted bioRxiv a license to display the preprint in perpetuity. It is made available under aCC-BY-ND 4.0 International license.

produce strains carrying an inserted gene cassette containing a constitutively expressed mCherry gene (this study). Cultures of *Ps* B728a and *Pf* A506 transformants were grown overnight in LB media, supplemented with either 30mg/mL gentamicin or 50mg/mL kanamycin respectively, under agitation of 400RPM at 28°C. Subsequently, the strains were diluted in sterile phosphate-saline buffer (PBS 1X, 137mM NaCl, 2.7mM KCl, 8mM Na_2HPO_4, and 2mM KH_2PO_4) and inoculated into 24-well plates containing leaf solution (LS) only or LS supplemented with natural leaf surface microbiota as described below.

Leaf surface microbiota extraction

Fresh leaves from a pear tree (*Pyrus communis*) and from greenbean plants (*Phaseolus vulgaris*) were sampled from organically grown plants (pear from Kiryat Malakhi area and bean from near Modi'in, Israel) in order to retrieve the microbiota associated with their surfaces. Both the abaxial and adaxial sides of the leaves were individually scraped using a disposable cell spreader after shallowly submerging a leaf in about 10mL sterile PBS while ensuring the petiole was not submerged in the solution. The scraped microbiota was then transferred to sterile 50ml Falcon tubes, and the remaining loosely attached microbes were re-suspended in about 1-3ml PBS 1X from the post-scraping leaf. All leaves utilized in this experiment were picked within 12h of microscope screens.

Leaf solution

Leaf solutions (LS) of both pear and green bean leaves were prepared separately by blending 2 to 4 leaves, depending on leaf size, in 500mL of PBS 1X. The resulting solution was then autoclaved and filtered through 0.2-µm filters (Millex-GV) to remove leaf particles and intact microbial cells.

Microscopic analysis of the spatial organization of cells and microbiota on the surface

Ps B728a and *Pf A*506 strains were grown overnight in LB media to a mid-log phase (OD_{600} 1.0). The culture OD was first adjusted to OD 0.5, and then further diluted by a factor of 1,000 in PBS (by employing serial dilutions). Leaf microbiota extractions (leaf wash) were diluted by a factor of between x5 to x10 to ensure that the microbiota density was not too high for the required spatial analysis (i.e., to ensure that the surface is not too densely covered by microbiota). Subsequently, 150µL of the leaf wash product containing the microbiota from either pear or bean leaves was gently

bioRxiv preprint doi: https://doi.org/10.1101/695734; this version posted July 8, 2019. The copyright holder for this preprint (which was not certified by peer review) is the author/funder, who has granted bioRxiv a license to display the preprint in perpetuity. It is made available under aCC-BY-ND 4.0 International license.

inoculated into 24-well plates (24-well glass bottom plate #1.5 high-performance cover glass 0.17±0.005mm, Cellvis, USA) containing 800µL of the corresponding LS (i.e., pear of green bean leaf solution) per well. Immediately after microbiota inoculation, the well plates containing the pear or bean systems were then inoculated with 50µL of diluted *Pf* A506 or *Ps* B728a. Cultures were subjected to time-lapse microscopic analysis under 40X magnification using the Eclipse Ti-E inverted microscope (Nikon, Japan). Imaging was performed at 30-min intervals covering a total area of 0.98mm^2 per well per time point (3x3 fields of views) using bright field, GFP, and RFP filters.

Image processing and segmentation of microbiota cells

We have used a combination of segmentation techniques. We used Ilastik , a machine learning image segmentation software (30), for the segmentation of the fluorescently tagged immigrant bacteria; and for the segmentation of microbiota cells and aggregates. RFP and GFP fluorescent channels of the microscope images were used to segment the *Pf* A506 cells and *Ps* B728a cells respectively. The bright field (BF) channel was used to segment the microbiota population. The segmentation process began with a manual training phase on a subset of images, until reaching a satisfactory classifier for isolating the objects in the image from the background. We used the classifier on all of the timepoints of our data, then surveyed the segmentation results for validation. The segmented cells found in the fluorescent channel were then removed from the BF images, leaving only the cells that originated in the leaf microbiota. In the segmentation of the *Pf* A506 images, which were tagged with RFP, microbiota RFP auto-fluorescence made it very challenging to automatically differentiate between microbiota and the fluorescently tagged cells. We eventually had to add a manual filtering stage to our automatic segmentation to differentiate between the tagged cells and the auto-fluorescent microbiota.

Statistical Analysis

The segmented microscopic images of the colonized surface were processed using MATLAB. To assess the statistical significance of the spatial proximity of the immigrant cells to microbiota cells and aggregates, the distribution of the minimal distances between immigrant cells and microbiota was compared with that estimated by a null random model (described below). The distances between immigrant cells

bioRxiv preprint doi: https://doi.org/10.1101/695734; this version posted July 8, 2019. The copyright holder for this preprint (which was not certified by peer review) is the author/funder, who has granted bioRxiv a license to display the preprint in perpetuity. It is made available under aCC-BY-ND 4.0 International license.

and microbiota aggregates were measured edge to edge, i.e., from the edge of the immigrant cell to the edge of the nearest microbiota aggregate.

The null random model is computed by randomizing the localization of all of the immigrant cellular components while preserving the shape and area of each such component. This randomization was done 99 times to generate a simulation envelope (15, 31, 32). For each such random localization of immigrant cells, the minimal distance between every immigrant cell (or aggregate) and the microbiota cells were computed, and a simulation envelope determined. The randomized localizations of all immigrant cells were restricted to non-microbiota-populated areas; extensions beyond the image area boundaries are not allowed. Whenever such a restriction was violated, a new random localization of the given cellular unit (cell or aggregate) was chosen (33).

The wide gray band in the Figs. That presents the spatial analyses represents the simulation envelope. In the above analyses, we considered immigrant cell clusters of any size (area) and microbiota objects of area > 6.4 μm^2 (equivalent to an area of 2 or more cells; this allowed us to remove solitary bacterial microbiota cells from this analysis). Using a higher threshold (than 6.4 μm^2) yielded a lower statistical significance.

To generate the null random model in the reciprocal analysis of the minimal distances of microbiota cells from newly formed aggregates of immigrant bacteria, the localization of the microbiota cells on the surface was randomized while preserving their shape and size. The minimal distances of cells or small cell clusters (cell clusters of size between 0.5 μm^2 to 6.4 μm^2; corresponding to clusters of up to ~2 cells) from immigrant bacteria aggregates (area > 8 μm^2 corresponding to > 2 cells) was computed. Using other size thresholds (for both immigrant bacteria aggregates and microbiota cells) yielded a lower statistical significance.

Results

A description of our experimental design is depicted in Fig. 1. Briefly, fresh leaves were picked from organically-grown open-field green bean plants (*Phaseolus vulgaris*) and from an organically-grown pear tree (*Pyrus communis*) (Fig. 1A). The

bioRxiv preprint doi: https://doi.org/10.1101/695734; this version posted July 8, 2019. The copyright holder for this preprint (which was not certified by peer review) is the author/funder, who has granted bioRxiv a license to display the preprint in perpetuity. It is made available under aCC-BY-ND 4.0 International license.

leaf surface microbiota of each plant was extracted as described below (Fig. 1C, Materials and Methods). In addition, to better represent the chemical environment of the leaf, leaf solutions (LS) were prepared for each plant species by blending fresh leaves (Fig. 1D; Materials and Methods). Fluorescently tagged *Ps* B728a or *Pf* A506 cells (Fig. 1B), which acted as the immigrant bacteria in our experiments, were inoculated into glass-bottom multi-well plates containing LS media, with and without the natural resident microbiota extracted from bean and pear leaves, and surface colonization was tracked through live imaging (Fig. 1E-F, Materials and Methods).

We first performed surface colonization experiments on *Ps* B728a or *Pf* A506 cells with LS only (i.e., without leaf microbiota cells) and tracked them under the microscope for 13 hours. Inoculation with bean LS led to a more rapid and intense surface colonization of both strains compared to pear LS (Fig. 2), possibly due to higher nutrient concentrations. Interestingly, per given plant LS, the strain whose plant was the native plant colonized the surface more rapidly. With bean LS, *Ps* B728a colonized the surface faster than did *Pf* A506; yet when pear LS was used, *Pf* A506 colonized the surface faster than did *Ps* B728a (Fig. 2). In addition, a clear difference was observed between the surface colonization patterns of the two strains: While *Pf* A506 commonly form aggregates on the well-surface, *Ps* B728a was observed mostly as solitary cells that covered the surface more homogenously (Fig. S1).

To extract the natural epiphytic microbiota from the leaf surface, we applied a protocol developed in our lab that is based on mechanical scraping (see Materials and Methods). This method preserved most small and mid-size (~50μm) aggregates intact, and efficiently recovered the majority of microbiota cells from the leaf surface. The leaf microbiota of both plants included bacteria, yeast-like cells, and fungi in both solitary and aggregated forms (as observed by microscopy, Fig. 3). Many of the aggregates were ‘mixed’, i.e., comprised of both bacteria and yeast cells. The bean microbiota was denser, and contained larger aggregates of up to ~50μm in diameter. The pear microbiota was less dense and contained smaller aggregates of up to ~30μm (Fig. 3).

To study how immigrant bacteria spatially organize on the surface in the presence of resident leaf microbiota, we first inoculated the wells with the leaf microbiota, with

bioRxiv preprint doi: https://doi.org/10.1101/695734; this version posted July 8, 2019. The copyright holder for this preprint (which was not certified by peer review) is the author/funder, who has granted bioRxiv a license to display the preprint in perpetuity. It is made available under aCC-BY-ND 4.0 International license.

the addition of its matching plant LS. We then inoculated *Ps* B728a or *Pf* A506 cells (the immigrant cells), as described in Materials and Methods, and tracked the respective surface colonization over time under the microscope (every 30 minutes for 13h). As time passed from the inoculation point, an increasing number of immigrant cells were observed on the well bottom surface (Fig. 4). Immigrant cells were observed attaching to the surface, moving, dividing, detaching, and some of them forming cell clusters (micro-colonies) in the form of surface-attached aggregates.

Next, we wanted to know whether and how the spatial organization of immigrant cells on the surface was affected by that of the resident microbiota cells. We first identified all microbiota components through image analysis. To that end, we applied machine learning techniques to segment the natural microbiota that consisted of morphologically distinct cells: bacterial, yeast, and fungal cells in both solitary and aggregated forms (Fig. 3, Materials and Methods). To exclude solitary microbiota cells from this analysis, we considered only microbiota components above a given size (> 6.4 μm^2, or equivalent to >2 cells, see Materials and Methods). The immigrant bacterial cells were identified based on their fluorescence signals. Then, we computed the distance from each immigrant cell cluster (a solitary cell or a micro-colony) to the closest microbiota component. We then compared these minimal distances' distributions to those expected by chance (Fig. 5). To do so, we randomized the localization of all immigrant cell clusters on the surface for each image (see Materials and Methods), and analyzed the minimal distances over 99 such random organizations to create simulation envelopes (31).

For all four combinations of immigrant strains and microbiota, the only distance range found to consistently deviate from random (i.e., outside of the simulation envelopes) was that of 0-2 μms (Fig. 6A-D). There were significantly more immigrant cell clusters within a distance < 2 μms to the closest microbiota component in comparison to this number than that expected by chance (see Materials and Methods). This means that immigrant bacteria preferentially attached to surface locations near microbiota cell clusters (defined as aggregates of > 2 cells) (Figs. 6E, F; Fig. S2).

To better understand the dynamics of the observed preferential attachment, we analyzed its deviation from random attachment over time. The number of *Ps* B728a cells within 2 μms distance from bean microbiota cells began to deviate from the

bioRxiv preprint doi: https://doi.org/10.1101/695734; this version posted July 8, 2019. The copyright holder for this preprint (which was not certified by peer review) is the author/funder, who has granted bioRxiv a license to display the preprint in perpetuity. It is made available under aCC-BY-ND 4.0 International license.

simulation envelope at around 5-7h post inoculation (Fig. 7A), and the deviation from random increased with time. At t = 13h there were 1355 cell clusters per mm^2 at a distance < 2 μms to microbiota cells, compared to 947 cell clusters ([872,1020] simulation envelope, n = 99) that were expected by chance. PA was also observed when *Ps* B728a was introduced to non-native microbiota (pear) (Fig. 7B). With *Pf* A506 cells, PA was observed much earlier, at t = 3h, and was somewhat more pronounced with the pear (native plant) microbiota: 40 cell clusters at t = 9h vs. 10 cell clusters expected by chance ([2,21] simulation envelope, n = 99), compared to the bean (non-native plant) microbiota: 170 cell clusters vs. 90 cell clusters expected by chance ([69,113] simulation envelope, n = 99) (Fig. 7C,D).

Interestingly, we also noticed that individual microbiota cells were observed joining newly formed aggregates of *Pf* A506 (Figs. 8A, B). This was also captured by statistical analysis, now performed on the opposite direction. For each *Pf* A506 aggregate (above 8 μm^2, equivalent to >~2 cells) we calculated the number of microbiota cells (size <6.4 μm^2, equivalent to up to ~2 cells; in order to discard aggregates from this analysis) within a 2μm distance, and compared it to that expected by chance. To that end, we performed randomization, this time of the microbiota cell clusters. We found that the number of pear (native plant) microbiota cells within a distance of < 2μm to an *Pf* A506 aggregate is significantly higher than that expected by chance: 195 cells vs. 55 ([32,80] simulation envelope, n = 99) at t = 13h. A similar picture was observed for the bean (non-native) microbiota: 345 cells vs. 188 ([158,216] simulation envelope, n = 99) at t = 9h (Fig. 8B). In contrast to *Pf* A506 cells, *Ps* B728a cells were not forming aggregates (Fig. 4) and PA of microbiota cells to *Ps* B728a cells or cell clusters was observed for neither the native or non-native plant microbiota (at least not within first 9h; Fig. S3).

Discussion

In summary, through live imaging and spatial analyses at microscale, we show that immigrant bacteria display a non-random spatial colonization pattern with respect to the spatial organization of natural resident leaf microbiota cells. This non-random organization is not necessarily observable by eye, but was revealed by a rigorous image and spatial analysis. As our simplified system excludes the heterogeneity of

bioRxiv preprint doi: https://doi.org/10.1101/695734; this version posted July 8, 2019. The copyright holder for this preprint (which was not certified by peer review) is the author/funder, who has granted bioRxiv a license to display the preprint in perpetuity. It is made available under aCC-BY-ND 4.0 International license.

natural leaf surfaces, this non-random organization must originate in interactions between the immigrant and resident microbiota cells. We found that immigrant bacterial cells preferentially attached to surface localizations near microbiota aggregates (at distances < 2 μms). PA was observed for both studied strains and with the microbiota of both native and non-native plants. In addition, a reciprocal PA of microbiota cells near newly formed immigrant bacterial aggregates was commonly observed in *Pf* A506, but not *Ps* B728a.

In a previous study, we used modeling and computer simulations to show that PA can be an efficient general surface colonization strategy for bacteria on 'patchily colonized' surfaces that are exposed to periodic stress such as desiccation, antibiotics, and predation (23). The present study provides experimental evidence of PA being a common bacterial colonization strategy, particularly within the phyllosphere, but likely in other surface-related microbial habitats. This finding supports previous indications of PA in an *in vitro* experimental system using a single bacterial strain(34) or environmental microbiota (35).

Interestingly, we found that PA is observed in both studied strains and for both cases of introduction to native and non-native microbiota. The two studied strains exhibited very different colonization behavior under the experimental conditions: While *Pf* A506 attached to the surface and formed aggregates, *Ps* B728a loosely attached to the surface, showed higher surface motility, and did not form aggregates (Fig. 4). This supports the view that PA is a general strategy that is not strain specific, and that PA can be implemented through diverse cell behaviors, e.g., *Pf* A506's biased surface attachment decisions near microbiota aggregates, or *Ps* B728a's gravitation toward microbiota aggregates via surface motility.

PA can be a result of both passive and active mechanisms. An example of a passive mechanism is the reported biased surface movement toward dense areas controlled by sticky trails of polysaccharide (34). Active mechanisms may involve chemotactic movement toward aggregates (36), which may underlie the observed gravitation of *Ps* B728a toward microbiota aggregates, or informed attachment decisions, which may in turn underlie *Pf* A506's observed PA near microbiota aggregates. Intra- and interspecies quorum sensing are possibly involved in such active mechanisms (36, 37), especially as quorum-sensing signals on unsaturated surfaces such as plant leaf

bioRxiv preprint doi: https://doi.org/10.1101/695734; this version posted July 8, 2019. The copyright holder for this preprint (which was not certified by peer review) is the author/funder, who has granted bioRxiv a license to display the preprint in perpetuity. It is made available under aCC-BY-ND 4.0 International license.

surfaces are highly localized, and quorum size can be surprisingly small, even as low as a few dozen cells (36, 38). Other sensing systems, such as peptidoglycan sensing by bacteria, can serve as indicators of cell proximity (39).

Regardless of the exact underlying mechanism, PA is an aggregate enrichment stratagem that leads to a rich-get-richer process, and thus may confer fitness advantage in environments that select for collective protection from stresses (23). Aggregates have been shown to increase bacterial cell survival on leaves under dry conditions (21, 40). In addition, aggregation has been found to increase survival on drying surfaces under moderate humidity through the formation of larger microscopic droplets around aggregates (41). These microdroplets have been shown to protect cells from desiccation (41). Immigrant bacteria that employ PA may have thus higher survival rates on the leaf surface, especially during their initial colonization period. This may lead to increased protection – provided by already-established microbiota aggregates – from the various stresses that cells experience on leaf surfaces, including desiccation, UV radiation, antibiotics, and predation.

It was not clear if the PA that we observed is toward specific members (e.g., species or strains) of the microbiota, or is broadly toward microbiota aggregates. As the leaf microbiota is comprised of hundreds of species, it is reasonable to assume that aggregates' specific species compositions affect PA behavior. Bacterial cells are known to sense their local environments, and cell colonization and behavior has been shown to be affected by interspecies signaling (42). Initial evidence for such interactions at the microscale, even between closely related strains within the same species, has been recently observed in isolated strains from the rhizosphere (43).

The spatial scales of interactions are of major importance in microbial ecology (15, 44). Our work indicates that the effective scale for such interactions is at distances < ~5μms. The number of immigrant bacterial cell clusters at distances > 4μms does not significantly deviate from random (Fig. 6). Interestingly, the increase in number of cell clusters at distance <2 μms from microbiota aggregates appears to come at the expense of cell clusters at the 2-4 μm range, and possibly at ranges up to ~10-20 μms for *Pf* A506, as can be seen by the smaller number of cell clusters than expected by random in that distance range (Figs. 6A-D). This tells us that the effective interaction

bioRxiv preprint doi: https://doi.org/10.1101/695734; this version posted July 8, 2019. The copyright holder for this preprint (which was not certified by peer review) is the author/funder, who has granted bioRxiv a license to display the preprint in perpetuity. It is made available under aCC-BY-ND 4.0 International license.

distance range is typically limited to a range < ~10 μms, consistent with the conclusions of previous work on bacterial interactions on leaf surfaces (15).

To conclude, our study demonstrates that microscale interactions between bacterial cells have a role in leaf microbiota surface colonization, and that two-way interactions between immigrant bacterial cells and resident microbiota are in play. In particular, preferential attachment of cells to bacterial aggregates is suggested to be a common surface colonization strategy that is expected to confer fitness advantage. In the broader picture, our results are likely relevant to many other surface-associated microbial habitats, including plant and animal microbiomes.

Acknowledgements

We thank Y Hadar for valuable comments on the manuscript. We thank S. Lindow for kindly providing bacterial strains, and R. Feuchtwanger from Gan Hasade and N. Shachar for providing fresh leaves for this study. JP acknowledges The Lady Davis trust for a postdoctoral fellowship. MB acknowledges the Rudin MSc scholarship. This work was supported by a research grant to N.K. from the James S. McDonnell Foundation (Studying Complex Systems Scholar Award, Grant #220020475).

bioRxiv preprint doi: https://doi.org/10.1101/695734; this version posted July 8, 2019. The copyright holder for this preprint (which was not certified by peer review) is the author/funder, who has granted bioRxiv a license to display the preprint in perpetuity. It is made available under aCC-BY-ND 4.0 International license.

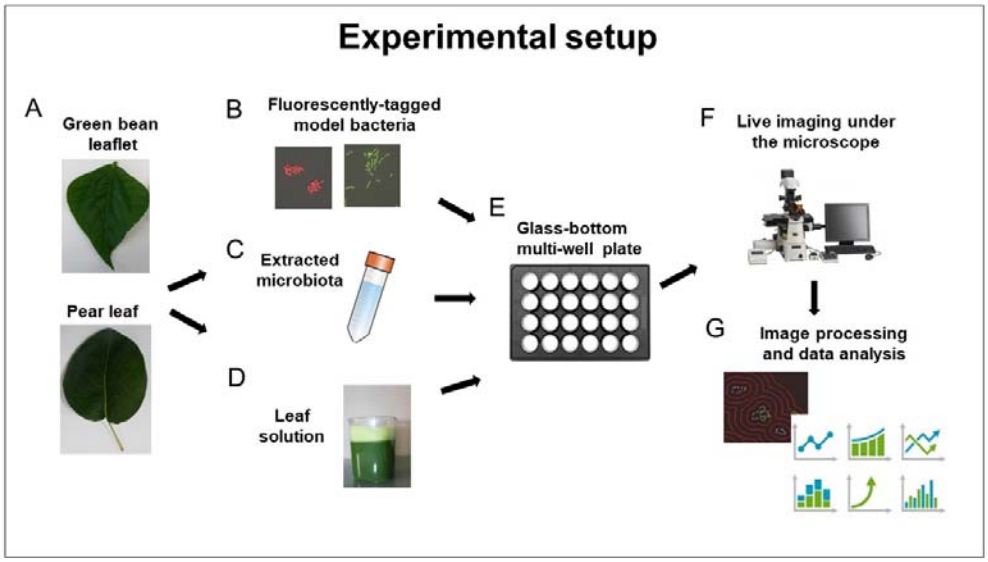

Fig. 1 Experimental Setup. A. Fresh green bean and pear leaves were picked. **B.** Fluorescently tagged *Ps* B728a and *Pf* A506 were used as immigrant bacteria. **C.** The natural microbiota was extracted from leaf surfaces **D.** Leaf solution was prepared from each plant. **E.** *Ps* B728a or *Pf* A506 were inoculated into glass-bottom wells with LS only or with both LS and microbiota. **F.** Surface colonization was tracked over time under the microscope. **G.** Image processing and data analysis were performed using custom software in MATLAB.

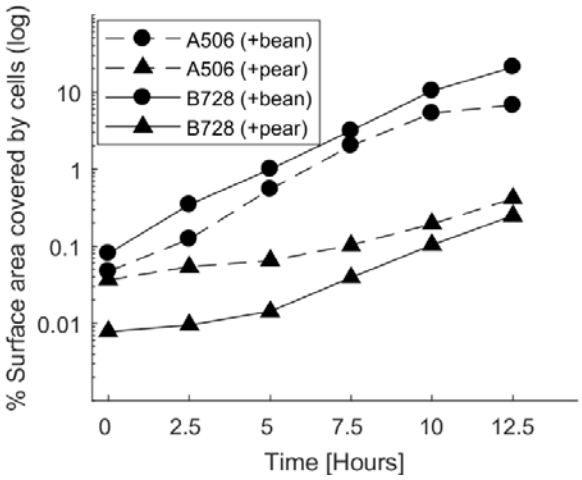

Fig. 2 Surface colonization dynamics without microbiota (leaf solution only). The graphs show the % of surface that is covered by cells as a function of time.

bioRxiv preprint doi: https://doi.org/10.1101/695734; this version posted July 8, 2019. The copyright holder for this preprint (which was not certified by peer review) is the author/funder, who has granted bioRxiv a license to display the preprint in perpetuity. It is made available under aCC-BY-ND 4.0 International license.

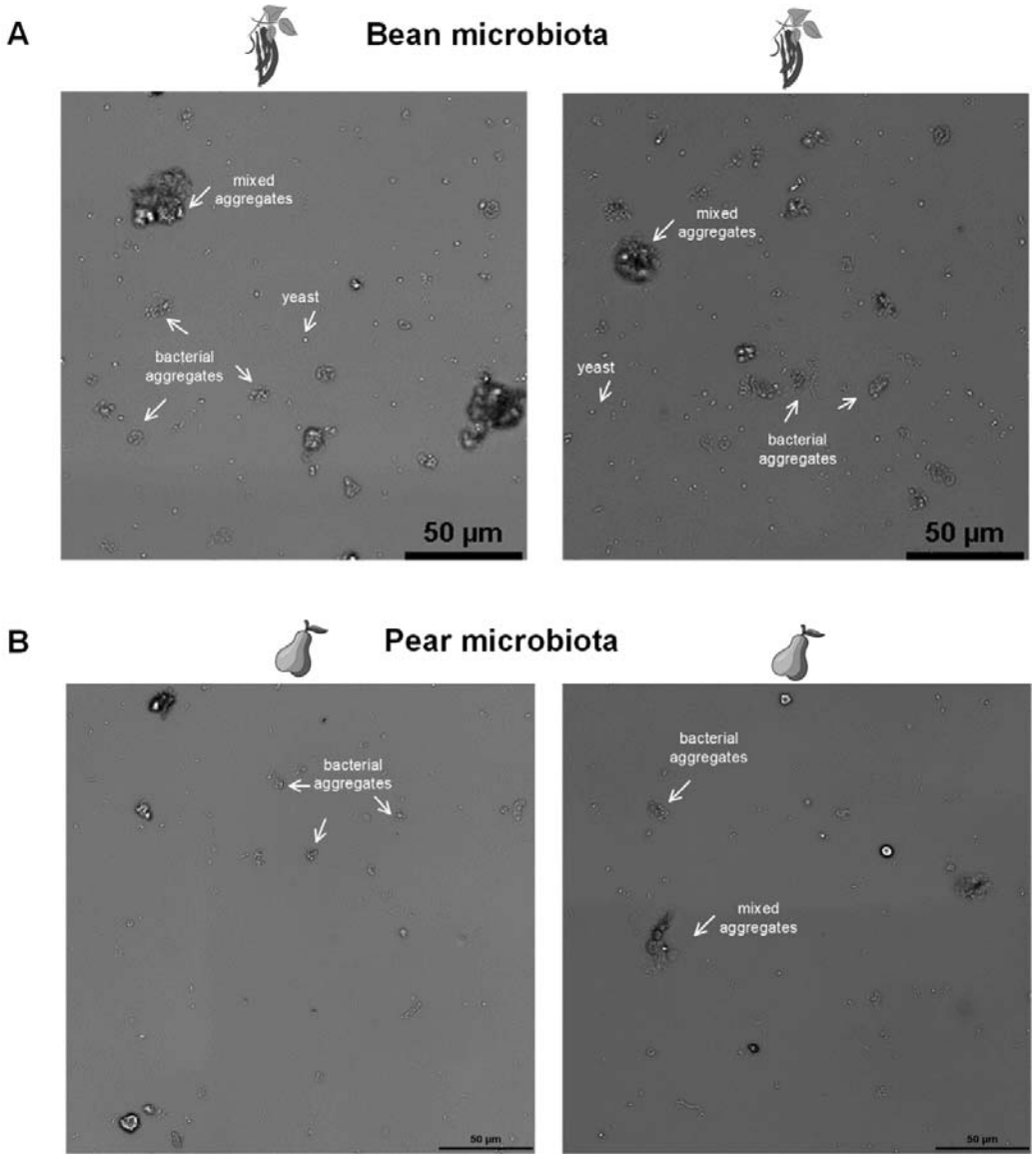

Fig. 3 Extracted microbiota from bean and pear leaves. Two representative images of the extracted microbiota from bean (**A**) and pear (**B**) leaf surfaces, as observed on glass-bottom well plates, prior to immigrant bacteria colonization.

bioRxiv preprint doi: https://doi.org/10.1101/695734; this version posted July 8, 2019. The copyright holder for this preprint (which was not certified by peer review) is the author/funder, who has granted bioRxiv a license to display the preprint in perpetuity. It is made available under aCC-BY-ND 4.0 International license.

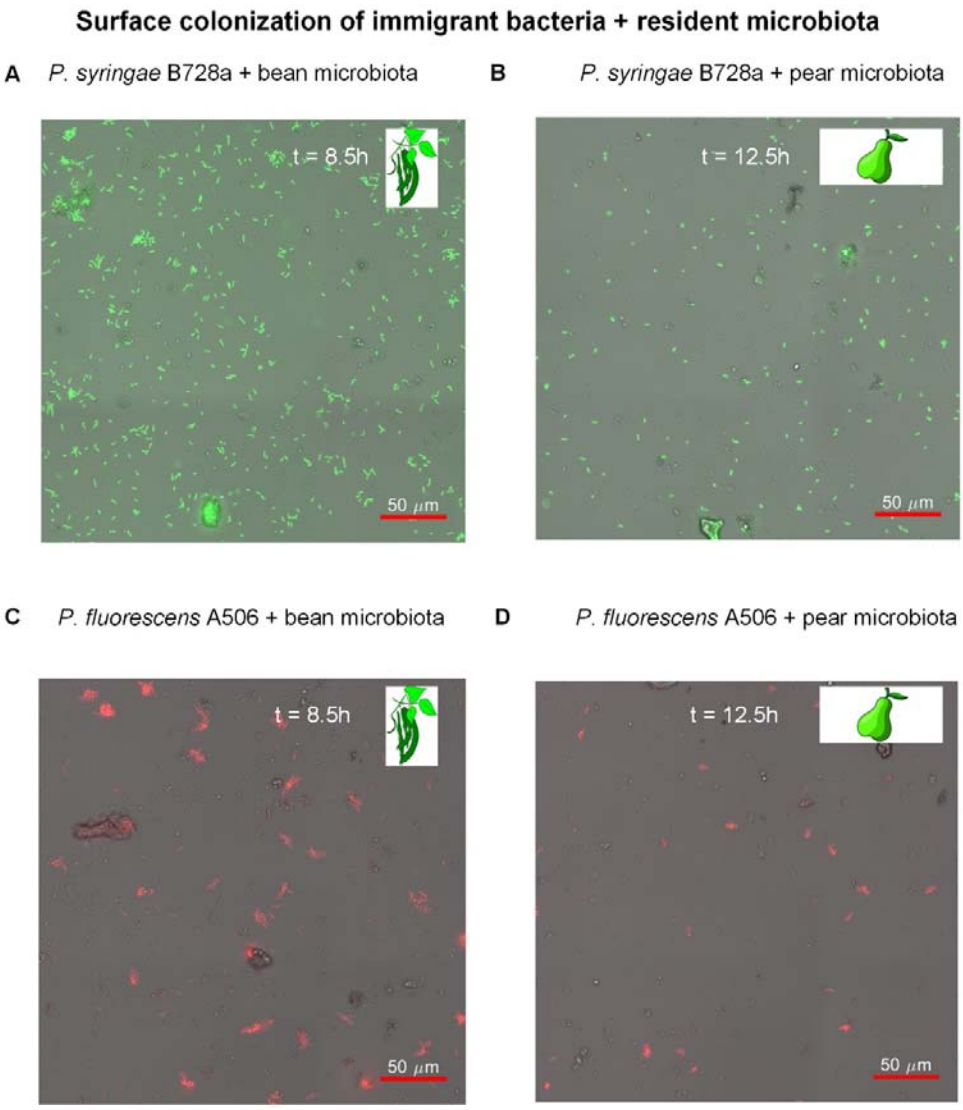

Fig. 4 Surface colonization of immigrant bacteria introduced to resident microbiota. A. *Ps* B728a with bean microbiota + LS (at t = 8.5h). **B.** *Ps* B728a with pear microbiota + LS (at t = 12.5h). **C.** *Pf* A506 with bean microbiota + LS (at t = 8.5h). **D**. *Pf* A506 with pear microbiota + LS (at t = 12.5h). Note the differing colonization patterns of the two strains: *Pf* A506 formed aggregates, while *Ps* B728a remained mostly as solitary cells that colonized the surface in a less 'clustered' pattern.

bioRxiv preprint doi: https://doi.org/10.1101/695734; this version posted July 8, 2019. The copyright holder for this preprint (which was not certified by peer review) is the author/funder, who has granted bioRxiv a license to display the preprint in perpetuity. It is made available under aCC-BY-ND 4.0 International license.

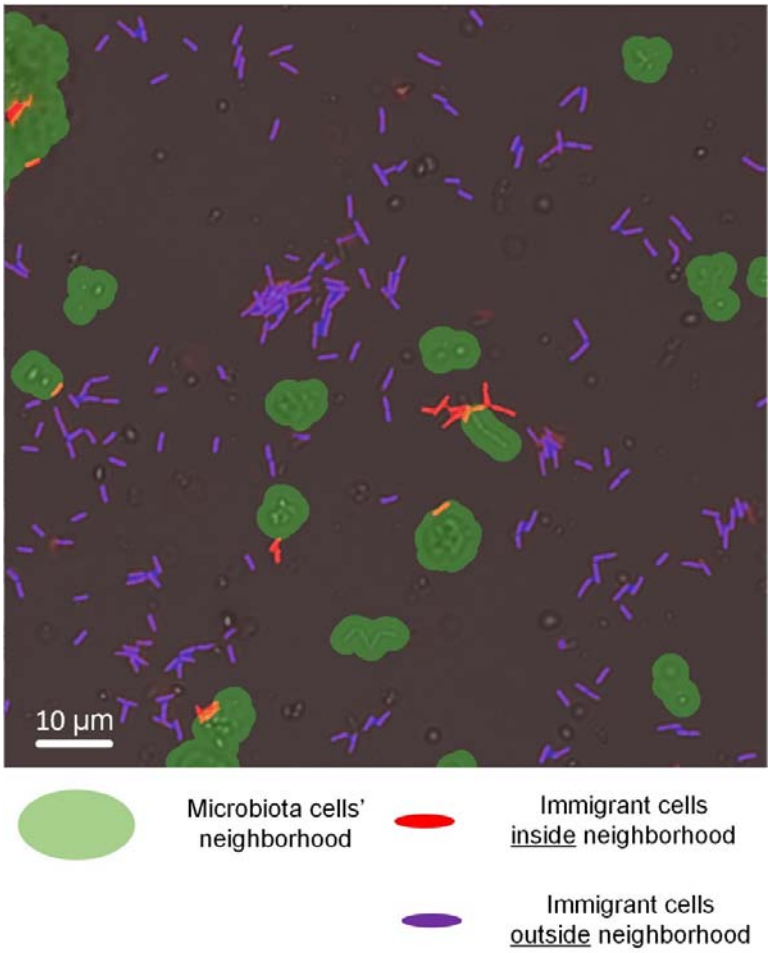

Fig. 5 Image analyses methodology. First, segmentation of all cellular objects and their classification (microbiota or immigrant bacteria) was applied. Then, for each immigrant cell cluster (either solitary cell or an aggregate of more than one cell), the distance to the closest microbiota entity was computed. The number of immigrant cell clusters for various distance ranges were calculated. As an example, in the image, all of the immigrant cell clusters within a distance of up to 2µms to its closest microbiota cluster are marked in red. The green area shows the 2-µm neighborhood of the microbiota cell clusters. Purple cells are immigrant cells outside this neighborhood (thus not counted in the distance range of 0 to 2µms). The number of cell clusters within a given distance range (i.e., 0 to 2 µms) was then compared to a simulation envelope that represented what is expected by chance only. Microbiota cells not highlighted in green are mostly solitary microbiota cells that were below the aggregate-size range that we considered in the analysis (> 6.4 μm^2).

bioRxiv preprint doi: https://doi.org/10.1101/695734; this version posted July 8, 2019. The copyright holder for this preprint (which was not certified by peer review) is the author/funder, who has granted bioRxiv a license to display the preprint in perpetuity. It is made available under aCC-BY-ND 4.0 International license.

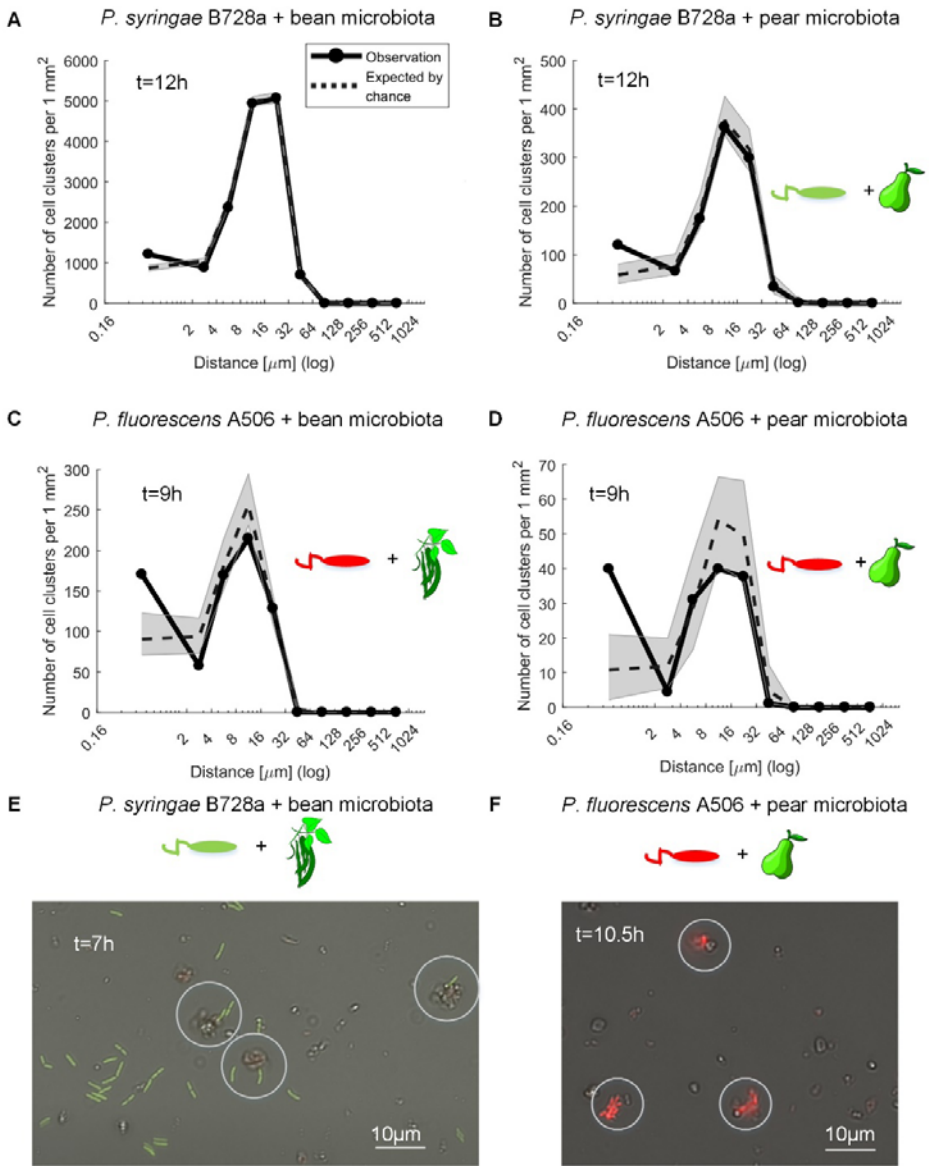

Fig. 6 'Distance profiles' of immigrant cell clusters with respect to microbiota cell clusters. The number of immigrant cell clusters (solitary cells or aggregates) as a function of minimal distances to closest microbiota aggregates (binned in logarithmic scales). Black solid line: the observed number; black dashed line: mean number as expected by chance (based on randomization of the locations of immigrant cells, see Materials and Methods). Grey: simulation envelope based on 99 randomizations. For all four combinations of immigrant strain and plant microbiota, the only "distance" range that showed a significant deviation from the expected is at distances of 0-2µms. **A.** *Ps* B728a + bean microbiota (native) at t = 12h. **B.** *Ps* B728a + pear microbiota (non-native) at t = 12h. **C.** *Pf* A506 + bean microbiota. (non-native) at t = 9h. **D.** *Pf* A506 + pear microbiota (native) at t = 9h. **E-F.** Microscope images showing attachments of immigrant cells near microbiota aggregates (white circles): **(E)** *Ps* B728a and bean microbiota and **(F)** *Pf* A506 and pear microbiota.

bioRxiv preprint doi: https://doi.org/10.1101/695734; this version posted July 8, 2019. The copyright holder for this preprint (which was not certified by peer review) is the author/funder, who has granted bioRxiv a license to display the preprint in perpetuity. It is made available under aCC-BY-ND 4.0 International license.

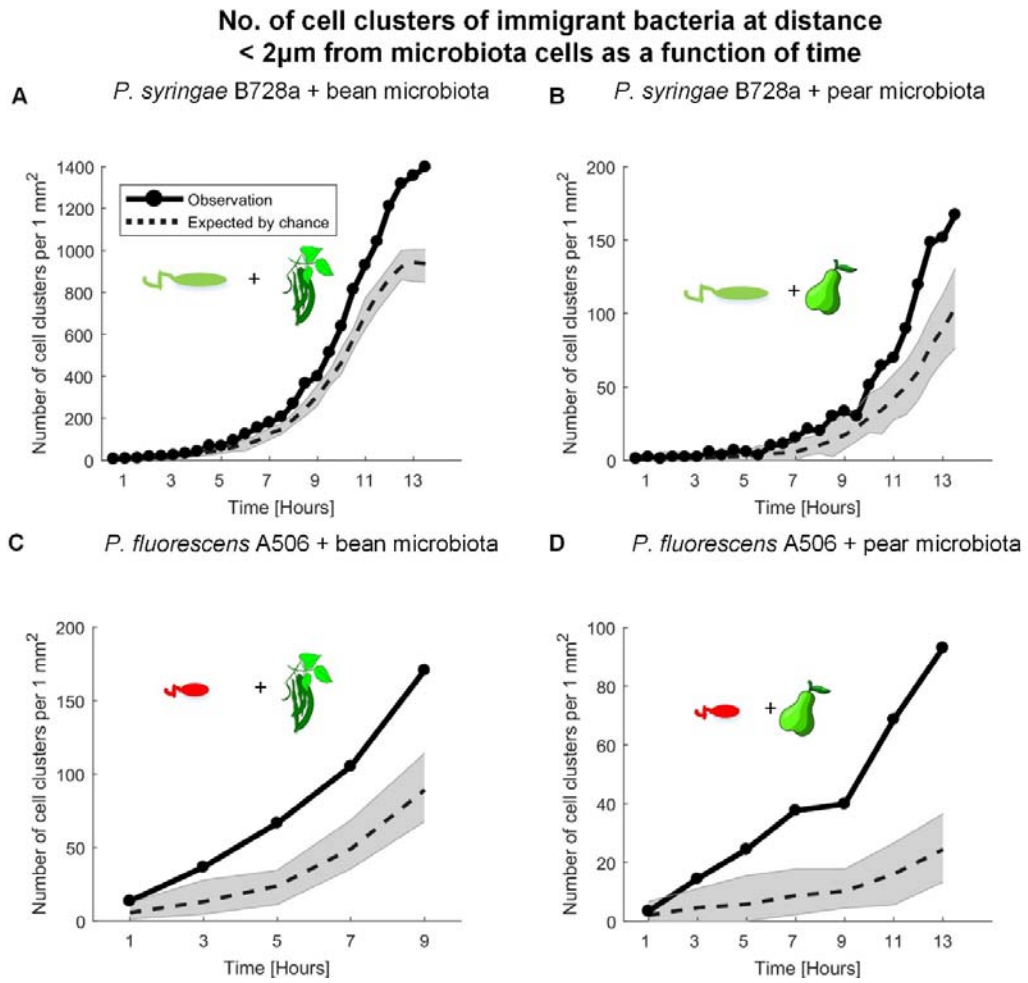

Fig. 7 Preferential attachment of immigrant cells near microbiota aggregates at various time points after inoculation. The graphs show the dynamics of the number of immigrant bacteria cell clusters at a distance < 2µms of microbiota aggregates over time. Black solid line: the observed number; black dashed line: mean number as expected by chance (based on randomization of the locations of immigrant cells, see Materials and Methods). Grey: simulation envelope based on 99 randomizations. In all cases at times later than t = 7h for *Ps* B728a and t = 3h for *Pf* A506, the number of cell clusters at a distance < 2µms from microbiota aggregates is significantly higher than that expected by chance. **A.** *Ps* B728a + bean microbiota (native). **B.** *Ps* B728a + pear microbiota (non-native). **C.** *Pf* A506 + bean microbiota (non-native). **D.** *Pf* A506 + pear microbiota (native).

bioRxiv preprint doi: https://doi.org/10.1101/695734; this version posted July 8, 2019. The copyright holder for this preprint (which was not certified by peer review) is the author/funder, who has granted bioRxiv a license to display the preprint in perpetuity. It is made available under aCC-BY-ND 4.0 International license.

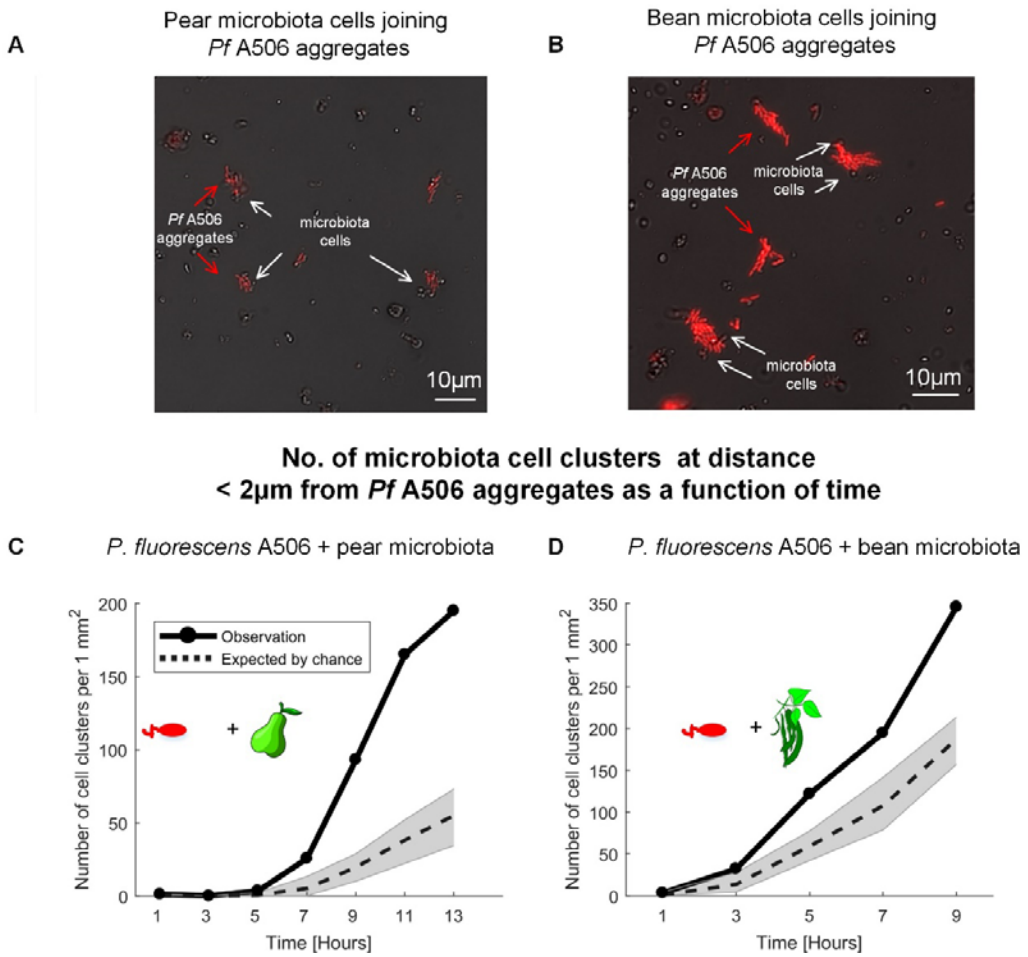

Fig. 8 The dynamics of preferential attachment of microbiota cells near newly formed *Pf* A506 aggregates. A-B. Microscopic image showing microbiota cells (A: pear; B: bean) that recently joined newly formed *Pf* A506 aggregates. **C-D.** The graphs show the dynamics of number of microbiota cells near *Pf* A506 aggregates over time (C: pear microbiota (native); D: bean microbiota (non-native)). Black solid line: the observed number; black dashed line: mean number as expected by chance (based on randomization of the locations of immigrant cells). Grey: simulation envelope based on 99 randomizations.

bioRxiv preprint doi: https://doi.org/10.1101/695734; this version posted July 8, 2019. The copyright holder for this preprint (which was not certified by peer review) is the author/funder, who has granted bioRxiv a license to display the preprint in perpetuity. It is made available under aCC-BY-ND 4.0 International license.

References

1. Lindow SE, Brandl MT. Microbiology of the phyllosphere. Appl Environ Microbiol. 2003;69(4):1875-83.
2. Lindow SE, Leveau JH. Phyllosphere microbiology. Current Opinion in Biotechnology. 2002;13(3):238-43.
3. Vorholt JA. Microbial life in the phyllosphere. Nature Reviews Microbiology. 2012;10(12):828.
4. Vacher C, Hampe A, Porté AJ, Sauer U, Compant S, Morris CE. The phyllosphere: microbial jungle at the plant–climate interface. Annual review of ecology, evolution, and systematics. 2016;47:1-24.
5. Bringel F, Couée I. Pivotal roles of phyllosphere microorganisms at the interface between plant functioning and atmospheric trace gas dynamics. Frontiers in microbiology. 2015;6:486.
6. Redford AJ, Bowers RM, Knight R, Linhart Y, Fierer N. The ecology of the phyllosphere: geographic and phylogenetic variability in the distribution of bacteria on tree leaves. Environmental microbiology. 2010;12(11):2885-93.
7. Rastogi G, Sbodio A, Tech JJ, Suslow TV, Coaker GL, Leveau JH. Leaf microbiota in an agroecosystem: spatiotemporal variation in bacterial community composition on field-grown lettuce. The ISME journal. 2012;6(10):1812.
8. Beattie GA, Lindow SE. Bacterial colonization of leaves: a spectrum of strategies. Phytopathology. 1999;89(5):353-9.
9. Agler MT, Ruhe J, Kroll S, Morhenn C, Kim S-T, Weigel D, et al. Microbial hub taxa link host and abiotic factors to plant microbiome variation. PLoS Biology. 2016;14(1):e1002352.
10. Laforest-Lapointe I, Messier C, Kembel SW. Tree phyllosphere bacterial communities: exploring the magnitude of intra-and inter-individual variation among host species. PeerJ. 2016;4:e2367.
11. Monier J-M, Lindow S. Frequency, size, and localization of bacterial aggregates on bean leaf surfaces. Appl Environ Microbiol. 2004;70(1):346-55.
12. Tecon R, Leveau JH. The mechanics of bacterial cluster formation on plant leaf surfaces as revealed by bioreporter technology. Environmental microbiology. 2012;14(5):1325-32.
13. Remus-Emsermann MN, Lücker S, Müller DB, Potthoff E, Daims H, Vorholt JA. Spatial distribution analyses of natural phyllosphere-colonizing bacteria on A rabidopsis thaliana revealed by fluorescence in situ hybridization. Environmental microbiology. 2014;16(7):2329-40.
14. Morris CE, Monier J, Jacques M. Methods for observing microbial biofilms directly on leaf surfaces and recovering them for isolation of culturable microorganisms. Appl Environ Microbiol. 1997;63(4):1570-6.
15. Esser DS, Leveau JH, Meyer KM, Wiegand K. Spatial scales of interactions among bacteria and between bacteria and the leaf surface. FEMS microbiology ecology. 2015;91(3):fiu034.
16. Remus-Emsermann MN, Schlechter RO. Phyllosphere microbiology: at the interface between microbial individuals and the plant host. New Phytologist. 2018;218(4):1327-33.
17. Monier J-M, Lindow S. Spatial organization of dual-species bacterial aggregates on leaf surfaces. Appl Environ Microbiol. 2005;71(9):5484-93.
18. Peredo EL, Simmons SL. Leaf-FISH: microscale imaging of bacterial taxa on phyllosphere. Frontiers in microbiology. 2018;8:2669.
19. Remus-Emsermann MN, Tecon R, Kowalchuk GA, Leveau JH. Variation in local carrying capacity and the individual fate of bacterial colonizers in the phyllosphere. The ISME journal. 2012;6(4):756.

bioRxiv preprint doi: https://doi.org/10.1101/695734; this version posted July 8, 2019. The copyright holder for this preprint (which was not certified by peer review) is the author/funder, who has granted bioRxiv a license to display the preprint in perpetuity. It is made available under aCC-BY-ND 4.0 International license.

20. Remus-Emsermann MN, Kowalchuk GA, Leveau JH. Single-cell versus population-level reproductive success of bacterial immigrants to pre-colonized leaf surfaces. Environmental microbiology reports. 2013;5(3):387-92.
21. Monier J-M, Lindow S. Aggregates of resident bacteria facilitate survival of immigrant bacteria on leaf surfaces. Microbial Ecology. 2005;49(3):343-52.
22. Poza-Carrion C, Suslow T, Lindow S. Resident bacteria on leaves enhance survival of immigrant cells of Salmonella enterica. Phytopathology. 2013;103(4):341-51.
23. Grinberg M, Orevi T, Kashtan N. Bacterial surface colonization, preferential attachment and fitness under periodic stress. PLoS computational biology. 2019;15(3):e1006815.
24. Beattie GA, Lindow SE. Comparison of the behavior of epiphytic fitness mutants of Pseudomonas syringae under controlled and field conditions. Appl Environ Microbiol. 1994;60(10):3799-808.
25. Loper JE, Lindow SE. Lack of evidence for the in situ fluorescent pigment production by Pseudomonas syringae pv. syringae on bean leaf surfaces. J Phytopathology. 1987;77(10):1449-54.
26. Wilson M, Hirano S, Lindow S. Location and survival of leaf-associated bacteria in relation to pathogenicity and potential for growth within the leaf. Appl Environ Microbiol. 1999;65(4):1435-43.
27. Stockwell V, Johnson K, Sugar D, Loper J. Control of fire blight by Pseudomonas fluorescens A506 and Pantoea vagans C9-1 applied as single strains and mixed inocula. Phytopathology. 2010;100(12):1330-9.
28. Wilson M, Lindow S. Interactions between the biological control agent Pseudomonas fluorescens A506 and Erwinia amylovora in pear blossoms. Phytopathology. 1993;83(1):117-23.
29. Choi K-H, Schweizer HP. mini-Tn7 insertion in bacteria with single attTn7 sites: example Pseudomonas aeruginosa. Nature protocols. 2006;1(1):153.
30. Sommer C, Straehle C, Koethe U, Hamprecht FA, editors. Ilastik: Interactive learning and segmentation toolkit. 2011 IEEE international symposium on biomedical imaging: From nano to macro; 2011: IEEE.
31. Baddeley A, Diggle PJ, Hardegen A, Lawrence T, Milne RK, Nair G. On tests of spatial pattern based on simulation envelopes. Ecological Monographs. 2014;84(3):477-89.
32. Ripley BD. Modelling spatial patterns. Journal of the Royal Statistical Society: Series B (Methodological). 1977;39(2):172-92.
33. Hanus ML, Hann DW, Marshall DD. Reconstructing the spatial pattern of trees from routine stand examination measurements. Forest Science. 1998;44(1):125-33.
34. Zhao K, Tseng BS, Beckerman B, Jin F, Gibiansky ML, Harrison JJ, et al. Psl trails guide exploration and microcolony formation in early P. aeruginosa biofilms. Nature. 2013;497(7449):388.
35. Hödl I, Hödl J, Wörman A, Singer G, Besemer K, Battin TJ. Voronoi tessellation captures very early clustering of single primary cells as induced by interactions in nascent biofilms. PloS one. 2011;6(10):e26368.
36. Laganenka L, Colin R, Sourjik V. Chemotaxis towards autoinducer 2 mediates autoaggregation in Escherichia coli. Nature communications. 2016;7:12984.
37. Laganenka L, Sourjik V. Autoinducer 2-dependent Escherichia coli biofilm formation is enhanced in a dual-species coculture. Appl Environ Microbiol. 2018;84(5):e02638-17.
38. Dulla G, Lindow SE. Quorum size of Pseudomonas syringae is small and dictated by water availability on the leaf surface. Proceedings of the National Academy of Sciences. 2008;105(8):3082-7.

bioRxiv preprint doi: https://doi.org/10.1101/695734; this version posted July 8, 2019. The copyright holder for this preprint (which was not certified by peer review) is the author/funder, who has granted bioRxiv a license to display the preprint in perpetuity. It is made available under aCC-BY-ND 4.0 International license.

39. Bertsche U, Mayer C, Götz F, Gust AA. Peptidoglycan perception—sensing bacteria by their common envelope structure. International journal of medical microbiology. 2015;305(2):217-23.
40. Monier J-M, Lindow S. Differential survival of solitary and aggregated bacterial cells promotes aggregate formation on leaf surfaces. Proceedings of the National Academy of Sciences. 2003;100(26):15977-82.
41. Grinberg M, Orevi T, Steinberg S, Kashtan N. Bacterial survival in microscopic droplets. bioRxiv. 2019; https://doi.org/10.1101/662437
42. Shank EA, Kolter R. New developments in microbial interspecies signaling. Current opinion in microbiology. 2009;12(2):205-14.
43. Nesli T, Orevi T, Grinberg M, Kastan N, Hadar Y, D M. Plant host affects bacteria-bacteria interactions. In preparation. 2019.
44. Schmidt H, Nunan N, Höck A, Eickhorst T, Kaiser C, Woebken D, et al. Recognizing patterns: spatial analysis of observed microbial colonization on root surfaces. Front Environ Sci. 2018;6:61.